

Neural dynamics of envelope coding

André Longtin^{a,b,c,*}, Jason W. Middleton^{a,b,c}, Jakub Cieniak^{a,b}, Leonard Maler^{a,c}

^a Center for Neural Dynamics, University of Ottawa, Ottawa, Canada

^b Physics Department, University of Ottawa, MacDonal Hall, 150 Louis-Pasteur, Ottawa, Ont., Canada K1N 6N5

^c Department of Cellular and Molecular Medicine, University of Ottawa, 451 Smyth Road, Ottawa, Canada

Received 5 December 2007; received in revised form 20 January 2008; accepted 25 January 2008

Available online 14 February 2008

Abstract

We consider the processing of narrowband signals that modulate carrier waveforms in sensory systems. The tuning of sensory neurons to the carrier frequency results in a high sensitivity to the amplitude modulations of the carrier. Recent work has revealed how specialized circuitry can extract the lower-frequency modulation associated with the slow envelope of a narrowband signal, and send it to higher brain along with the full signal. This paper first summarizes the experimental evidence for this processing in the context of electroreception, where the narrowband signals arise in the context of social communication between the animals. It then examines the mechanism of this extraction by single neurons and neural populations, using intracellular recordings and new modeling results contrasting envelope extraction and stochastic resonance. Low noise and peri-threshold stimulation are necessary to obtain a firing pattern that shows high coherence with the envelope of the input. Further, the output must be fed through a slow synapse. Averaging networks are then considered for their ability to detect, using additional noise, signals with power in the envelope bandwidth. The circuitry that does support envelope extraction beyond the primary receptors is available in many areas of the brain including cortex. The mechanism of envelope extraction and its gating by noise and bias currents is thus accessible to non-carrier-based coding as well, as long as the input to the circuit is a narrowband signal. Novel results are also presented on a more biophysical model of the receptor population, showing that it can encode a narrowband signal, but not its envelope, as observed experimentally. The model is modified from previous models by reducing stimulus contrast in order to make it sufficiently linear to agree with the experimental data.

© 2008 Elsevier Inc. All rights reserved.

Keywords: Neural coding; Integrate-and-fire model; Hilbert transform; Coherence; Electroreceptors; Stochastic resonance

1. Introduction

Many senses receive input in the form of amplitude or phase modulated carrier signals. This is the case for auditory systems throughout the animal kingdom. It is also the case for primary receptors in the electric sense of weakly electric fish [27]. The close similarity of coding principles between the electrosensory and auditory systems has been discussed in the literature [6]. For example, in the auditory system, the primary auditory receptors are tuned

to specific carrier frequencies. Information about stimuli is relayed to higher brain via both the frequency content, i.e. which carriers are present, and the time-varying modulations of the amplitude and phase of these carriers. The electrosensory system is essentially a simplified version of the auditory system when the fish is alone, since the receptors are driven by only one carrier. However, in the presence of other fish, the situation resembles the auditory system even more, in that different carriers are present along with their respective modulations.

While we focus herein on processing in the electrosensory system, the principles and mechanisms outlined below are applicable to other sensory systems where carriers are involved, as well as systems without carriers. These electric fish have a specialized organ in the tail that generates a

* Corresponding author. Address: Physics Department, University of Ottawa, MacDonal Hall, 150 Louis-Pasteur, Ottawa, Ont., Canada K1N 6N5.

E-mail address: alongtin@uottawa.ca (A. Longtin).

quasi-sinusoidal discharge throughout the life of the animal. The frequency of this electric organ discharge, or EOD, is very stable. The resulting oscillating field causes an oscillating voltage drop across the apical membrane of the specialized cutaneous “tuberous” receptors, which in turn drives neurotransmitter release onto afferent nerves. The resulting discharge pattern in these nerves is called the spontaneous (or baseline) activity because this situation corresponds to baseline conditions.

Distorsions of the amplitude and/or phase of this field caused by stimuli alter the baseline voltage oscillations, which in turn perturb the spontaneous discharge of the receptors [3,18]. This is “active” electrolocation, in contrast to passive electroreception that relies on ampullary receptors which many fish possess (including extraordinary sensitive ones as in the shark). The challenge is to understand how this basic active mode of sensation can allow a nervous system to encode and respond to a range of different stimuli, all of which must go through the electroreceptors. The eyes are of little use since they are nocturnal and live in turbid waters, and they can perform these tasks without vision. In other words, these receptors are the front end, and must deal with all incoming signals. The next layer of cells, known as pyramidal cells, then do the triage on these inputs, sending the appropriate features to the appropriate structures, with the help of interneurons as we will see.

This paper focusses on one mechanism that rises to the task of deciphering mixtures of signals: envelope extraction from narrowband signals. We discuss the biophysical mechanisms that underlie this extraction, and how it relates to single cell properties such as mean firing-vs-input bias ($f-I$) characteristics and noise level. We show how circuitry can convey a narrowband signal from one station to the next along with its associated low frequency envelope. The relation between this mechanism and suprathreshold/subthreshold firing, and ghost stochastic resonance in particular [10], is examined. The circuitry needs a cell that responds to the frequencies in the narrowband, but funnels its output through a lowpass inhibitory synapse. Such circuitry is found in many areas of cortex, and may explain our ability to extract, and thus perceive, higher order features from narrowband signals, such as those associated with superposition of gratings in the visual system [2,19] or speech recognition [15,23].

We further discuss how this envelope extraction and transmission can be gated by the noise and the bias. Since the extraction leads to power at low frequency, the question arises as to whether this power acts as a baseline noise that masks another signal – such as a prey – that has power in the same band as the extracted envelope. The analysis of this situation, carried out in detail here, leads to an interesting effect of signal-to-noise enhancement by noise in the context of an averaging network of such cells. This effect is different from stochastic resonance, since it is seen for a range of values around threshold. Finally we consider extraction in an even more biophysically realistic context,

namely by simulating the behavior of the afferents. As we will see, these spike trains have special noise-reducing properties at low frequencies, due to correlated firing seen in each cell.

The paper is organized as follows. Section 2 explains how different time scales of signals can arise using the electrosensory system, and provides background on the circuitry of this sensory system and its response to these signals of different time scales. Section 3 summarizes experiments and analyses of envelope extraction in this sense, after defining input-output coherence and Hilbert transforms. Section 4 discusses this mechanism in the context of a leaky integrate-and-fire model (LIF) with narrowband input, and shows the ranges of important parameters that allow extraction (“envelope gating”). Gating is didactically reviewed and further analyzed in the context of an averaging network of cells. It is important to realize that our analyses go beyond calculating transmission or extraction of signals using spectral measures, since they rely on coherence calculations, which can be used to provide a lower bound on rates of mutual information transmission. Finally, we present more biophysically realistic computational results of stimulus and envelope coding in the afferents, a first step in modeling the process up to the pyramidal cells and beyond.

2. Multiple time scales of stimuli

It is possible to illustrate the challenges that face sensory systems with carriers by focussing on electroreception. Further, understanding how the different signals are extracted in a carrier-based sense can yield principles for non-carrier-based senses too, such as vision [19,20]. In the electrosensory context there are different classes of stimuli. Prey and navigational cues such as rocks and plants provide low frequency (<20 Hz) input to the receptors. Tail bending, fin, gill and other body motions also fall in that range. Then there are social cues. When two fish are in the vicinity of one another, they each perceive a beat pattern that results from the superposition of the EOD's. The beat frequency is equal to the difference of the two EOD frequencies. In the brown ghost knife fish (*Apteronotus leptorhynchus*) the EOD is in the range of 500–750 Hz for females, and 800–1000 Hz for males. The presence of a beat signifies to each fish that another fish is present, and its frequency informs about the gender. This can lead to a change in the EOD frequencies according to a protocol known as the jamming avoidance response (JAR) which varies across the multitude of weakly electric fish species [14].

The next level of complexity involves active communication signals, in which the fish briefly modulate their EOD frequency. Same-gender interactions lead to so-called *small chirps* in the brown ghost, which are 20 ms increases in EOD frequency with little changes in EOD amplitude. Cross-gender interactions produce *large chirps*, of similar duration, but which are large increases in EOD frequency with a concomitant collapse in EOD amplitude [4].

Finally, there is the situation where many fish swim in the same area. It has been shown that they prefer to swim around in small groups of 6–8 individuals under natural conditions (Eric S. Fortune, personal communication). This leads to a superposition of 6–8 EOD's with time-varying amplitudes at the surface of each fish. Spectrograms of these signals show that they are narrowband, i.e. possess spectral power at all the differences of frequencies present in the mix. Strictly speaking, this power appears as sidebands of the EOD's, but we will neglect the EOD's for the sake of discussion and concentrate on these lower difference-frequencies. In fact, the high frequency EOD's are not transmitted, but leave their imprint in phase locking in the afferents and a certain subset of their projection cells (the deep basilar pyramidal cells).

The combination of difference-frequencies is an example of a narrowband signal, and it represents the basic “cocktail party” that the fish must decipher (see Fig. 1) – although it seemingly is further complicated by chirps, which we do not address here. Further, such narrowband mixtures have even slower amplitude-modulation components, which as we will see can be extracted by the Hilbert transform. For example, a 40–60 Hz narrowband Gaussian noise will display amplitude modulations in the 0–20 Hz range. This is a property of any narrowband signal, independent of whether this signal arose from beats between high frequency components (such as EOD's in the electro-sensory context). In contrast, the singular narrowband case of a single harmonic signal (e.g. a fish alone) does not show this amplitude modulation (instead it has constant amplitude), while a broadband signal does not have a well-defined slower modulation either.

Of course, the natural environment where fish are navigating, eating and interacting with other fish provides a natural mixture of all the cases above. Not only are the fish subjected to a cocktail party effect due to their proximity, but they also see other confounding signals that presumably limit their ability to separate out stimuli. Understanding the neural circuitry that implements this separation is within reach, and holds great promise for helping humans faced with similar challenges when they have sensory impairments.

3. Experimental envelope extraction

3.1. Methods

The signals we are interested in coding are narrowband (e.g. 40–60 Hz) amplitude modulation of the EOD. Our approach [20,21] consists in quantifying the linearity of the encoding of (1) the direct narrowband power into the spike train, and (2) the envelope of this waveform (extracted using the Hilbert transform) into the spike train. The coherence $C_{XY}(f)$ between an input signal X and an output signal Y is used to quantify this encoding. It is a function of frequency and varies between 0 for no linear encoding and 1 for perfect linear encoding:

$$C_{XY}(f) = \frac{|S_{XY}(f)|^2}{S_{XX}(f)S_{YY}(f)}, \quad (1)$$

where S_{XY} is the cross-spectral density between X and Y , and S_{XX} and S_{YY} is the autospectral density of X and Y , respectively. In our context, the input is an analog narrowband stimulus $S(t)$ and the output is the spike train of the cell or model,

$$R(t) = \sum_i \delta(t - t_i), \quad (2)$$

where the sum is over all the spike times. This leads to the stimulus–response (S–R) coherence C_{SR} . We will also consider the envelope–response (E–R) coherence C_{ER} between the envelope of the stimulus $E(t)$ and the spike train response, $R(t)$. We note that the cross-spectrum is related to the perhaps more familiar transfer function. However, the coherence further divides by the power of the output and thus is similar to a signal-to-noise ratio. It can be related simply to a lower bound measure of mutual information.

The envelope of the stimulus is extracted via the analytic signal technique, which associates with a real signal $x(t)$ an imaginary part $y(t)$; this latter part contains components phase shifted by 90° using the Hilbert transform $H[x(t)]$ [23,20,13]:

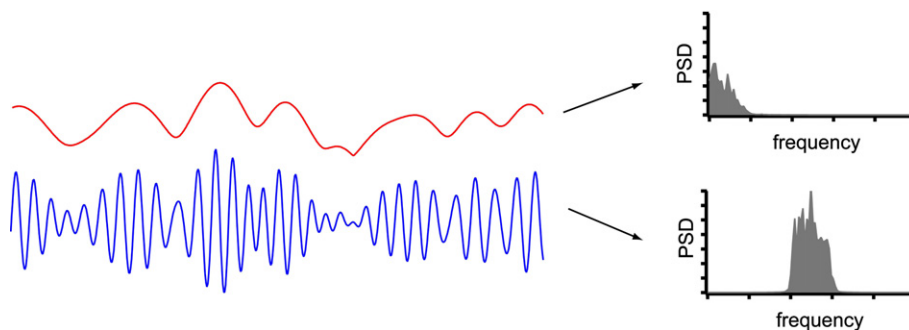


Fig. 1. A sample realization of 40–60 Hz Gaussian noise (blue) will give an envelope (red) with power in the 0–20 Hz range. Their power spectral densities are shown on the right in the bottom and top panels, respectively. (For interpretation of the references to colour in this figure legend, the reader is referred to the web version of this article.)

$$y(t) \equiv H[x(t)] = \frac{1}{\pi} P \int_{-\infty}^{\infty} \frac{x(\tau)}{t - \tau} d\tau, \quad (3)$$

where P means the Cauchy principal value. In the case of the narrowband signals that we use, the radial component of the corresponding analytic signal has an intuitive interpretation. This component is $A(t) = \sqrt{x^2(t) + y^2(t)}$, and represents the instantaneous amplitude or “signal envelope” that arises from the interference of spectral components with similar frequencies. It is this amplitude that forms the envelope signal.

3.2. Direct and indirect pathways

The first stages of the electrosensory pathway are organized as follows. The electrorereceptors are spread all over the body of the fish; homology to the sense of touch is obvious. They are more concentrated in the head region, which has been designated as the electrosensory fovea, although from measurements and modeling of the electric field lines around the body it is not clear whether the resolution is actually higher there than in the midbody region [1]. The afferents that innervate the receptor cells excite pyramidal cells in the electrosensory lateral line lobe (ELL). From there these excite the torus semi-circularis (TS), as well as the nucleus pre-eminentialis (Np) [5]. The latter feeds back to ELL (direct feedback) via both excitatory and inhibitory pathways. The torus massively feeds back to Np (the polarity of this connection is not fully established), which feeds back to ELL as we have just mentioned. Np also excites the cerebellar structure known as the EGP, which feeds back to ELL (indirect feedback) again via both excitatory and inhibitory pathways. The projections from receptors to ELL are spatially topographic. A local stimulus such as a prey affects a small part of the skin by causing field line distortions (if its impedance differs from that of the water); this in turn affects a few pyramidal cells. A global stimulus such as a beat and other communication signals affects all receptors and thus pyramidal cells, though not equally.

These receptor-to-ELL feedforward projections will be referred to as direct projections.

The receptors also excite interneurons known as ovoid cells. These cells have very large receptive fields, meaning that their firing rate changes only when global stimuli change. These ovoid cells display very good S–R coherence $C_{SR}(f)$ up to high frequencies (200 Hz or so when 0–200 Hz modulations are given), which suggests that they are made to process broadband input. Fig. 2 shows a spike train measured *in vivo* from an ovoid cell in response to a narrowband 40–60 Hz modulation of the EOD. As mentioned earlier in relation to Fig. 1, we see here that such input actually has a well-defined mean frequency, and a slower random “envelope” modulation. Spikes tend to occur on the crests of this input, as well as on crests of the envelope.

When given narrowband input such as 40–60 Hz, it shows very good S–R coherence in this range (and of course approximately zero coherence outside this range). It turns out that this cell also has excellent E–R coherence C_{ER} under the same conditions. The data, not shown, are similar to those shown for a pyramidal cell in Fig. 3. Pyramidal cells thus show, like ovoids, good S–R and E–R coherence, at least for global signals. Interestingly, this is not the case for the P-unit receptor that projects to both the ovoid and the pyramidal cell (not shown). These receptors behave too linearly (a fact demonstrated in [26,24]) to be able to extract any envelope, as we will see that this requires nonlinearity [20,10].

Where do the pyramidal cells get the ability to respond to the low-frequency envelope of the signal? Not from the receptor cells, since they do not have this property. Another clue comes from Fig. 4: if the stimulus is local, they lose their ability to respond to the envelope. And another clue still: the ovoids project to the pyramidal cells, although through a slow $GABA_B$ inhibitory synapse. Such a projection has been considered paradoxical, since the ovoids can respond to very high frequencies, but certainly can not transmit high-frequency information through such a slow bottleneck. The conclusion is that the ovoids actually extract the envelope, which allows them to have good E–R coherence. They further pass on the slow envelope to

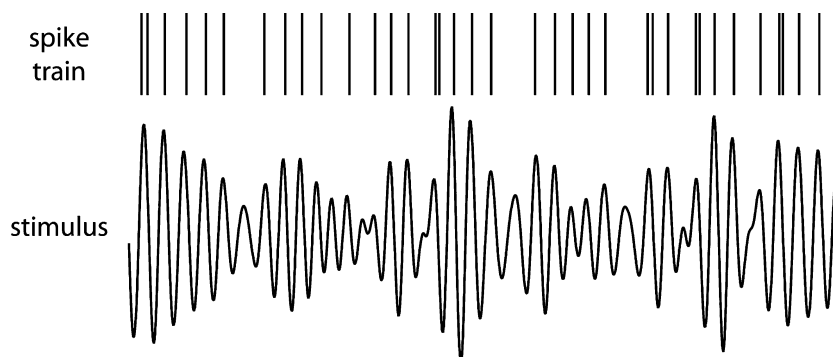


Fig. 2. A sample of the 40–60 Hz amplitude modulation given to an electric fish (bottom) and the spike train response of an ovoid cell recorded in the ELL.

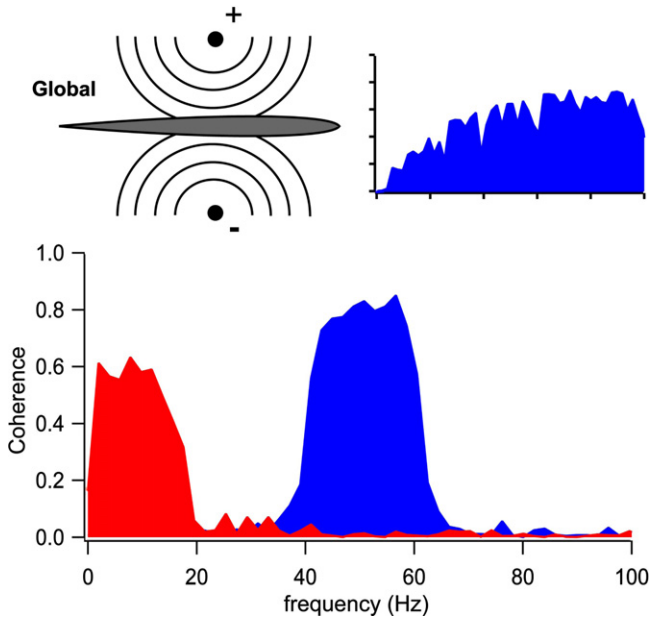


Fig. 3. In global stimulus geometry an E-type pyramidal cell, as expected, has high pass filtering characteristics when stimulated with broadband, 0–100 Hz, Gaussian noise (inset). S–R coherence is shown in blue, while E–R coherence is shown in red. (For interpretation of the references to colour in this figure legend, the reader is referred to the web version of this article.)

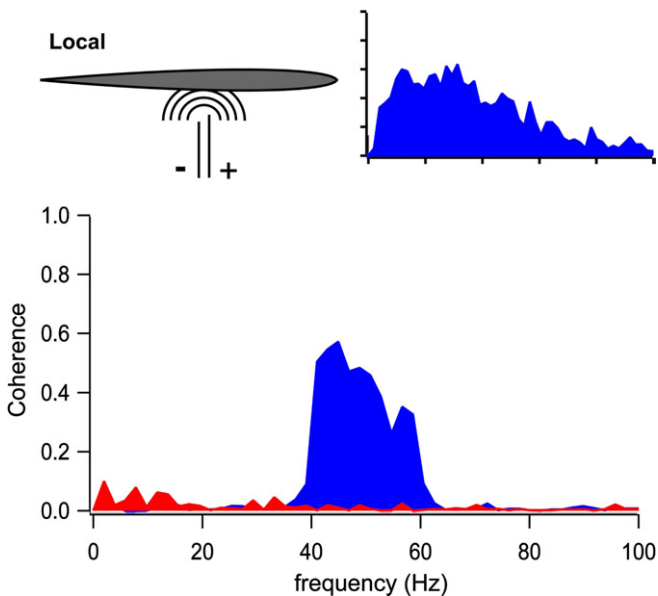


Fig. 4. In local stimulus geometry an E-type pyramidal cell has low pass filtering characteristics when stimulated with broadband, 0–100 Hz, Gaussian noise (inset). S–R coherence is shown in blue, while E–R coherence is shown in red. (For interpretation of the references to colour in this figure legend, the reader is referred to the web version of this article.)

the pyramidal cell through the slow synapse. This is why the pyramidal cell exhibits good E–R coherence. In fact, the pyramidal cell responds well to both the direct narrowband signal as well as its envelope, and presumably

the next stations such as torus and Np use the part that they need for processing. It has also been shown that the feedback pathways to the pyramidal cell do not provide the E–R response ability [20].

This circuitry, involving a direct feedforward excitatory projection and an indirect projection via an interneuron with a $GABA_B$ synapse, is present in many parts of the brain, including cortex. Hence envelope extraction, also known as higher-order feature extraction, can be supported in those areas. We next look at the conditions for such extraction at the single cell level; this in turn leads to a prediction of effects at the network level.

4. Modeling single cell envelope gating

In another study [21] we have explored the biophysics of envelope extraction from narrowband signals. This was done using an *in vitro* preparation rather than the *in vivo* preparation discussed up to now. The *in vitro* situation is free from potential confounding effects due to circuitry and synapses. One can focus on the single cell properties that allow envelope extraction. More specifically, this was done by injecting the narrowband stimulus directly into the cell. For technical reasons, this is easier to explore in pyramidal cells from *in vitro* slice preparations of the ELL – even though our results stated above point to the ovoids (presynaptic to these cells) as the cells that actually perform this extraction *in vivo*. Our results reveal generic biophysical aspects of this extraction procedure.

It has long been suggested that rectification plays an important role in extraction [12,19]. The f – I curve of a neuron has a natural rectification at rheobase: signals above threshold can modulate the firing rate, while those below are cut out. Fig. 5 shows this situation for a narrowband stimulus of interest, using an adiabatic assumption in which the (perhaps stochastic) firing rate instantaneously tracks changes in the injected current bias. Note however that the EOD is no longer present hereafter – we deal just with the narrowband signal injected intracellularly, as well as its associated low-frequency envelope. Fig. 5 shows that when the input signal straddles rheobase, the output firing rate has a low-frequency envelope. This would not be the case if the whole signal was mapped into firing rate using a linear part of the curve to the right of rheobase, i.e. for a higher bias: the absence of rectification would yield small fluctuations in the firing rate, and no envelope would be present.

Fig. 6 shows a caricature of the expected power in the spike train of a neuron in response to a narrowband input. The direct signal power in the input appears in the output. Because of nonlinearity, power at the harmonics of the narrowband is also seen, and the more so the stronger the rectification is, i.e. the more nonlinear the f – I curve is. We also see the envelope power at low frequency, with roughly the same bandwidth as the direct signal. Hence, this power in the output will depend on the nonlinearity, which is affected mainly by the bias current (distance to rheobase)

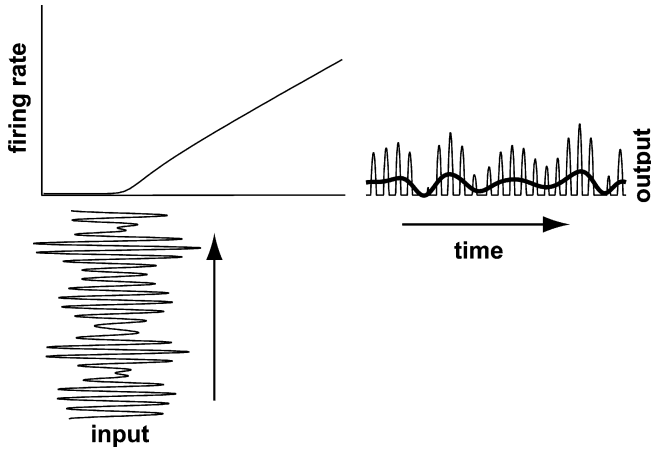


Fig. 5. A narrowband signal drives the input bias to a neuron near rheobase. The F–I curve acts as a static transfer function, mapping the signal to a time-varying firing rate. Under these conditions, the output firing rate (top right) is a rectified version of the input (bottom left). This envelope is seen here using a running average of the output rate over the fast time scale (thick line).

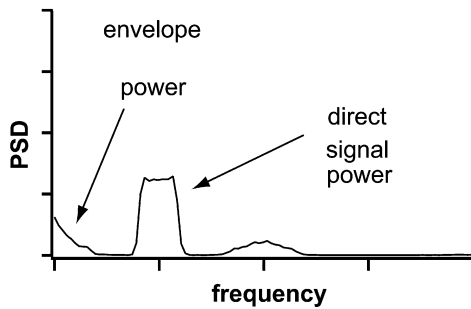


Fig. 6. The spectral power of the rate in Fig. 5 contains the same narrowband frequencies as the input, as well as the low frequencies of the slow time-varying envelope of this input.

and the noise which linearizes the f–I curve (see e.g. [11]). A linear system would not produce any output at frequencies not present in the input.

We now show how S–R and E–R coherence depend on these parameters using the leaky integrate-and-fire neuron model. This analysis has been shown to explain the experimental data from the pyramidal cells with *in vitro* current injection [21]. The model is

$$\tau \frac{dV}{dt} = -V + I + \sqrt{\frac{2D}{\tau}} \xi(t) + S(t), \quad (4)$$

where $S(t)$ is the injected narrowband signal and $\xi(t)$ is Gaussian white noise. The S–R coherence averaged over the frequency range of the narrowband signal for this model follows a sigmoidal shape, increasing from zero to one as the bias is increased, as expected (see [11,21] and references therein). It can be greater than zero even for subthreshold stimuli via noise-induced firing (stochastic resonance occurs in this range as we show below).

However, this sigmoidal behavior is not seen for the E–R coherence. Fig. 7 shows two examples of spike trains from this model, one for a bias near threshold, and the other above threshold. In this latter case many firings are seen, but not necessarily in a manner that encodes the amplitude of the envelope into an instantaneous firing rate

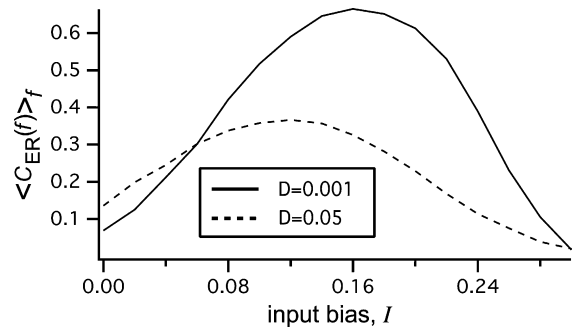


Fig. 8. The averaged values of envelope-response (E–R) coherence C_{ER} over the frequency range of the narrowband signal as a function of input current for $D = 0.001$ and 0.05 . The effect of stochastic resonance (SR) can be seen for small input bias values, i.e. additional noise increases input–output coherence. Otherwise, additional noise decreases E–R coherence.



Fig. 7. A sample of the 40–60 Hz amplitude given to a LIF neural model (top) and the spike train responses when the input bias is set at rheobase (middle) and in the suprathreshold regime (bottom).

(i.e. not clearly in a rate-coding manner). Fig. 8 shows rather a unimodal shape of C_{ER} as a function of the bias current, i.e. as a function of the parameter that sets the operating point of the neuron (the mean rate). The best C_{ER} occurs near rheobase, where rectification is strong. Below rheobase, there is not much firing to represent an envelope; above it, the system behaves more linearly, so C_{ER} is low. Further, Fig. 8 shows that as the noise increases, there is a drop in the quality of the linear encoding of the envelope (C_{ER}) for suprathreshold biases. On the other hand, an increase is seen for subthreshold biases. This latter effect where coherence increases with noise is stochastic resonance [11]. Together these two effects of noise and bias could have been predicted from the results on ghost stochastic resonance in the context of superposition of two or more harmonics of a signal (but without the fundamental) [10].

Fig. 9 plots C_{ER} versus the intensity of the internal noise, for both a subthreshold and suprathreshold bias. The external stimulus strength is held fixed. In the subthreshold case, the E–R coherence is insensitive to noise for lower noise intensities. A resonance is seen for moderate noise intensities, and the curve joins up with the one for the suprathreshold case at higher noise intensities. This stochastic resonance seen here for a narrow band of frequencies [11] is a consequence of noise-induced firing in the system for subthreshold stimuli, such that the noise assists in coding the input – without noise there would be spikes only for large positive excursions of the narrowband stimulus, and consequently poor representation of this signal and low coherence. We also see a simple monotonic decay of coherence in the suprathreshold bias case, starting from C_{ER} values that are higher than for the subthreshold case. Increasing noise thus removes E–R coherence. The resonance reflects what is seen below threshold (leftmost part)

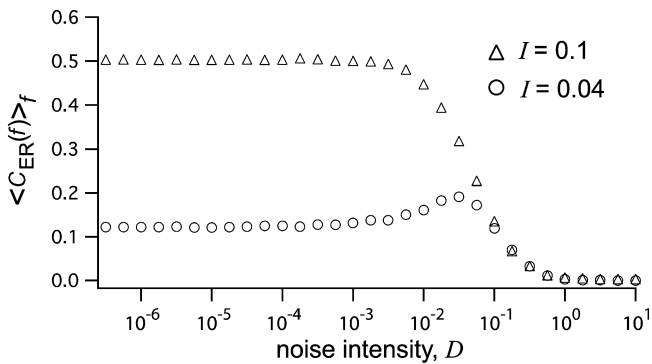


Fig. 9. Coherence between the spiking output and the envelope of the narrowband input averaged over the frequency range of the band as a function of noise intensity. The open triangles show the E–R coherence when the input of the LIF is set at rheobase ($I = 0.1$). The monotonic decreasing property of the ER-coherence in this firing regime shows that there is no conventional stochastic resonance (SR). The open circles show the E–R coherence when the neuron is in the subthreshold regime. The peak of ER-coherence between $D = 0.01$ and $D = 0.1$ indicates that, as expected, the system exhibits stochastic resonance in the deep subthreshold regime.

in Fig. 8, while the monotonic decay reflects the suprathreshold case in Fig. 8.

5. Modeling network envelope gating

5.1. Summing or averaging?

The motivation for this section comes from the observation that the power in the envelope, resulting from the proximity of other fish, lies in the same low frequency range as that associated with prey and navigational cues. Consequently, in the presence of other fish, any envelope power will lower the detectability of such prey and cues. How can these fish detect them when they live alongside other fish? More generally, one can also ask whether any new features appear when summing networks are processing narrowband input.

Perhaps if the noise level increases, the envelope detection will diminish, lowering the noise floor at low frequencies; other signals in that range could then be detected better. This is indeed the case, but only relative to the other spectral features such as the direct power in the narrowband range (not shown; see [21]); in absolute terms, the noise has gone up everywhere because there is just more firings, many of which are uncorrelated with the input. In other words, adding noise causes the whole spectrum to shift upward. Intuitively, this can be understood by the fact that the high-frequency limit of the spike train power spectrum is given by the mean firing rate (see e.g. [17]). A stimulus of constant strength, such as a 10 Hz sinusoidal signal, would still be hard to detect given the increase in the noise floor, and thus decrease in the signal-to-noise ratio.

An averaging network would normalize this summed input by a $1/N$ factor:

$$R_{\text{avg}}(t) = \frac{1}{N} \sum_j^N \sum_i \delta(t - t_i^j) \quad (5)$$

where t_i^j is the i -th firing time of the j -th neuron. Such averaging is often assumed in neural network theory (see e.g. [25]). The common assumption is one of synaptic normalization, where the strength of a synapse onto a postsynaptic neuron goes as the inverse of the total number of synapses onto this neuron. What then happens to the noise floor when the spiking outputs are summed and divided by N ? Fig. 10 shows the resulting power spectrum of such an averaged response $R_{\text{avg}}(t)$, obtained using N LIF neurons in parallel. Each LIF has the same narrowband input, but has its own internal noise source $\xi_j(t)$. Spectra are shown for two intensities of the intrinsic noise. Note that the bias is at rheobase. For both cases, the spectra show power in the narrowband, as well as at harmonics of that band, and at the envelope frequencies. This is similar to Fig. 6 using the spectral power of the rate of firing (from a single neuron), rather than the spike train as is used here. But for higher noise, the envelope power is much reduced, as are

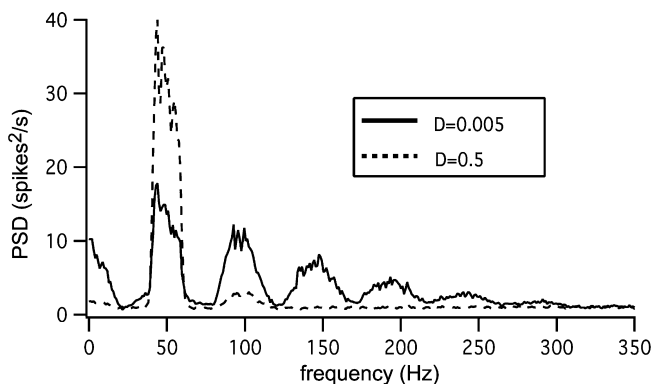


Fig. 10. The power spectral density of the average spike train, $R_{\text{avg}}(t)$, with $N = 50$ identical LIF neurons with independent uncorrelated noise for $D = 0.005$ (dashed line) and $D = 0.5$ (solid line). The noise floor at low frequencies is paradoxically reduced with the addition of intrinsic noise, so that the power of a small amplitude, low frequency harmonic input (as in Fig. 12) is more visible.

the harmonics of the narrowband. The stronger noise has linearized the f - I curve of each cell; these cells are no longer able to produce information at the envelope frequencies.

5.2. Suprathreshold gating resonance

Let us now insert a low frequency signal that falls in the band associated with envelope power. Fig. 11 shows that the signal rises above a higher noise floor (lower SNR) when the noise is weak than when it is strong (note that the signal peak is the same in both cases). This leads us to vary the noise intensity to see how the SNR behaves. Results are shown for a single neuron and for an averaging network of $N = 50$ neurons in Fig. 12. Apart from statistical fluctuations, the result for the single cell show a monotonically decreasing SNR. This is consistent with Fig. 9, where at rheobase, the increased noise decreases the E - R coherence. However, the whole spectrum shifts upward because of the increased firing rate; the net result is an increased noise floor, and decreasing SNR. However, for

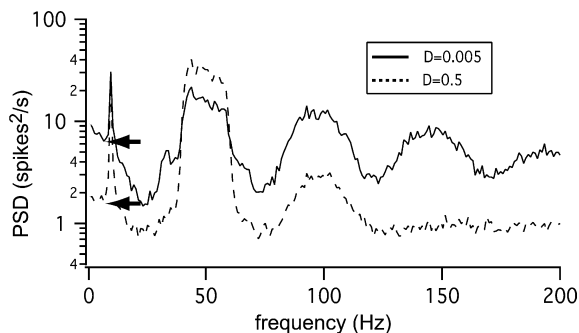


Fig. 11. The power spectral density of the average spike train, $R_{\text{avg}}(t)$, with $N = 50$ identical LIF neurons with independent uncorrelated noise for $D = 0.005$ (solid line) and $D = 0.5$ (dashed line), in the presence of an additional low frequency harmonic input at 10 Hz. The noise floor is indicated by the arrow in both cases.

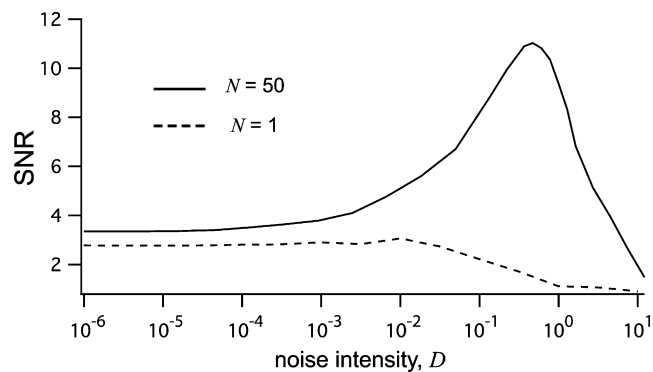


Fig. 12. The SNR of the averaged spike train, $R_{\text{avg}}(t)$, measured at the frequency of the sinusoidal input signal (10 Hz), shows a non-monotonic behavior as a function of noise intensity, D (solid line). This effect is due to the noise shaping that results from an increased intrinsic (and uncorrelated) noise followed by network averaging. This phenomenon is different than stochastic resonance, as demonstrated by the SNR curve for the single unit with the same parameters (dashed line). There is no strong non-monotonic behaviour of the SNR as a function of noise intensity.

the averaging network, the SNR is non-monotonic as a function of noise intensity, and there is in fact an optimal noise to detect the 10 Hz signal. The increased noise washes out the nonlinearity in the f - I curve, reducing envelope power. Yet the total power of the summed spike trains increases because all cells are firing more. Then the averaging brings the noise floor back down, and we see a good signal detection.

For the single cell, we discussed how noise and bias current can determine the strength of the envelope power, i.e. how they can *gate* the presence of the envelope in the output. Here, for an averaging network, one finds an optimal noise to detect a signal in the same band as the envelope. Noise can then gate the strength of this signal component by getting rid of the competing envelope. This effect is not stochastic resonance, as it is not limited to subthreshold inputs, neither for the narrowband nor the harmonic signal. Rather, it is seen in the neighborhood of rheobase where envelopes can be encoded in the first place, i.e. where E - R coherence is good (Fig. 8).

6. Gating in the presence of realistic synaptic input

Here we begin an investigation into a biophysically more realistic analysis of envelope gating. Ultimately we would like a model of the whole sensory periphery with the relevant circuitry and spiking dynamics. The precise details to include should be dictated by the problem under investigation. For envelope gating, it seems important to understand how the spiking of the receptor afferents can support the envelope extraction, as they are the main vehicle for information about the input that is used by the ovoid cells. Specifically, as discussed in Section 3.2, it has been shown [20] that the spike trains from the receptor afferents show good coherence with the narrowband signal, but not with its envelope.

The model for a single p-unit electroreceptor afferent is based on our earlier modeling studies [7] based in part on the earlier probabilistic model in [22]. The more recent implementation in [9] was first used because parameters are adjusted in a way that the threshold recovery after spiking produces negative correlations between successive interspike intervals, and the model displays the proper highpass filtering, without explicitly putting in this filtering as in [22]. The equations read

$$I_i(t) = [S(t) + A_0] \sin(2\pi f_{\text{EOD}}t) \Theta[(S(t) + A_0) \sin(2\pi f_{\text{EOD}}t)] \times [1 + \sigma \zeta_i(t)] \quad (6)$$

$$\tau_V \frac{dV_i}{dt} = -V_i + I_i \quad (7)$$

$$\tau_\theta \frac{d\theta_i}{dt} = \theta_0 - \theta_i \quad (8)$$

where $I_i(t)$ is the input to the i -th receptor, V_i is its transmembrane potential, and θ_i its time varying threshold for firing. A firing event occurs when the voltage meets the threshold. After each spike, the voltage is reset to zero, and the threshold is incremented by a fixed amount $\Delta\theta$. So the memory of past firings is conveyed via the threshold, which allows for non-renewal firing. A long interval will tend to be followed by a short and vice-versa. This is a deterministic property of the system [8], which is expressed by the noise. σ controls the intensity of the intrinsic neuronal white noise ζ . $S(t)$ is the narrowband signal, and f_{EOD} is the frequency of the EOD. The parameters chosen produce a spike on 20 percent of the cycles.

While this model provides good baseline statistics, we have found that it does not reproduce the experimental results on envelope coding. We have found (not shown) that it produces both good S–R and E–R coherence. We hypothesized that the reason for this is that it is operating

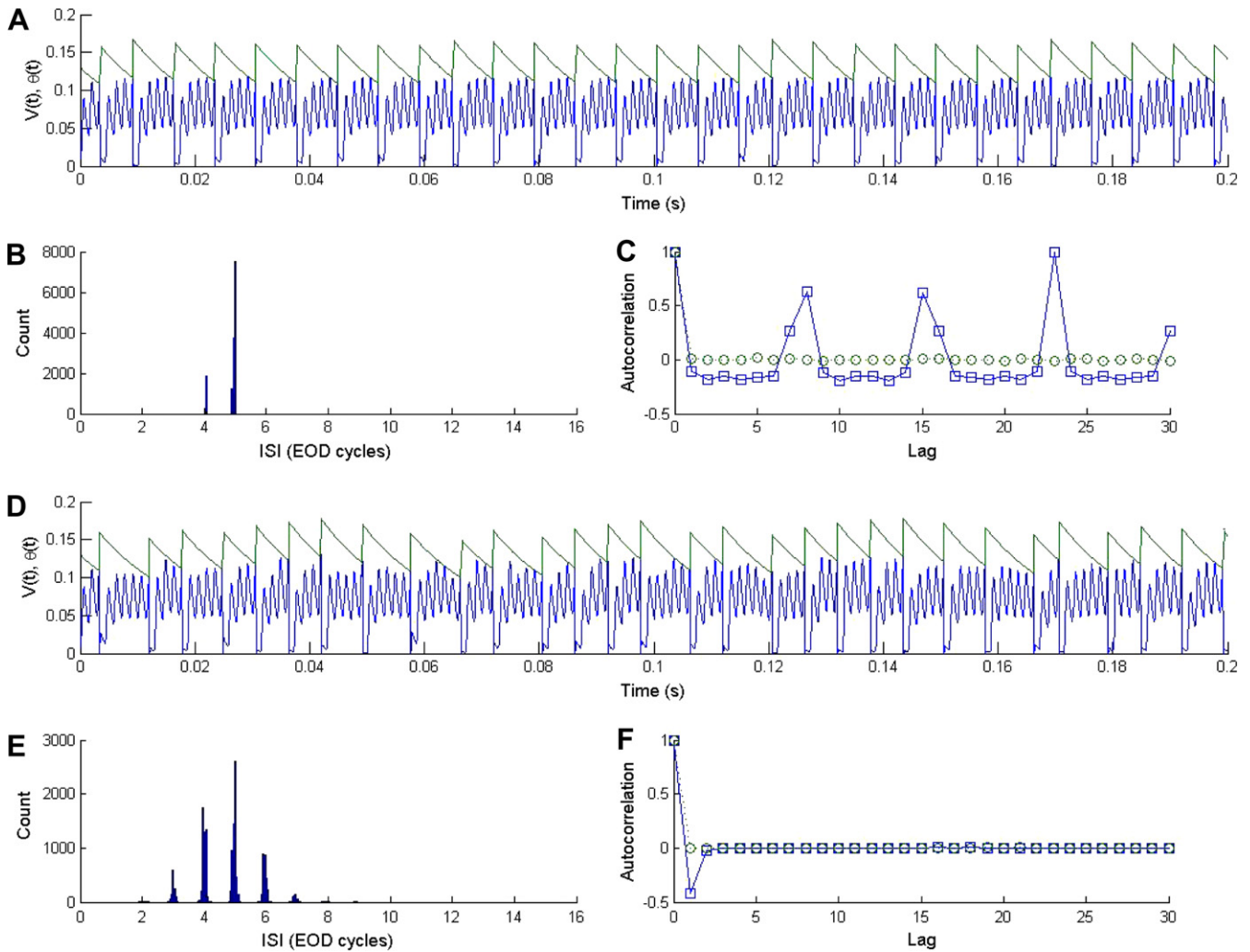


Fig. 13. Simulation (for 100 s) of baseline P-unit membrane potential using a leaky integrate-and-fire model with dynamic threshold producing data at a sampling rate of 20 kHz. Baseline means that there is no input signal other than the constant-amplitude EOD. (A–C) Internal noise intensity $\sigma = 0$. (D–F) Same as in (A–C) but with $\sigma = 0.002$. (A and D) Membrane potential, $V(t)$, and threshold, $\theta(t)$. (B and E) Interspike interval histogram obtained from (B) 1 realization and (E) 20 realizations, with time measured in EOD cycles. (C and F) Interspike interval autocorrelation (squares) and autocorrelation of shuffled ISIs (circles). Parameters used: $\tau_V = 1$ ms; $\tau_\theta = 14.5$ ms; $f_{\text{EOD}} = 700$ Hz; $A_0 = 0.2613$ mV; $\theta_0 = 0.03$ mV; $\Delta\theta = 0.05$ mV.

too much in a nonlinear regime. Our results thus predict that parameters that produce the baseline statistics and envelope coding (i.e. lack thereof) require a more linear P-unit. This can be achieved by increasing the noise and bias (into the suprathreshold regime) and decreasing the stimulus contrast (in comparison to [8]). Other properties still agree with experimental results (interval histogram and interval correlation – Fig. 13E and F). We present our results in the following Figures. In the last one (Fig. 15) we contrast results from a more linear and a less linear model, to show that nonlinearity can bring on good envelope coding.

In the absence of intrinsic noise this model exhibits a complex phase locking pattern made mostly of 6–7 intervals of 5 EOD cycles followed by an interval of 4 EOD cycles, as shown in Fig. 13A. Such phase locking patterns are expected from such models [7], and the interval distribution and the correlation between successive interspike

intervals is highly structured (Fig. 13B and C). Fig. 13D–F shows the same model but with intrinsic noise with a level that produces stochastic phase locking with realistic interval distributions and interval correlation [7], in particular, the negative correlation at lag one (long and short intervals alternate statistically).

Fig. 14 shows the response of the afferent model to a narrowband signal and to its envelope. The firing rate of the P-unit is increased slightly (spikes on 22 percent of the cycles as opposed to 20 without the modulation), as expected [24], and the interval histogram is broader. One also sees Fig. 15 plots the S–R and E–R coherence for a single cell, averaged over many presentations of the same frozen-narrowband-noise stimulus, for two different stimulus contrasts (stimulus standard deviation divided by EOD amplitude). The averaging is possible because the P-unit does not respond the same way to the same signal, due to its intrinsic noise which differs across realizations. It is

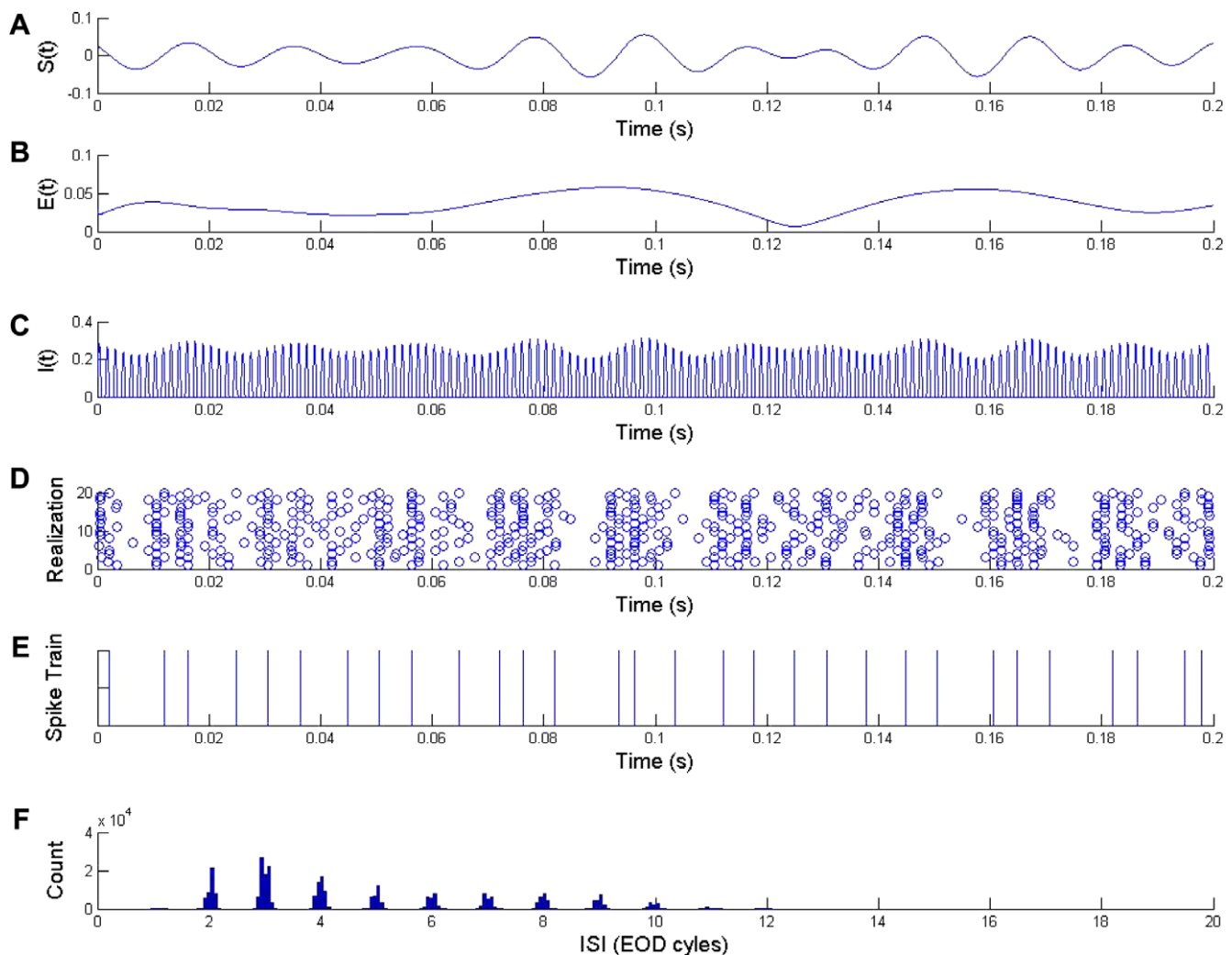


Fig. 14. Simulation with EOD amplitude-modulating stimulus, $S(t)$, taken as a narrowband Gaussian noise process with power in the 40–60 Hz range with standard deviation at 15% of EOD amplitude. (A) Stimulus, $S(t)$. (B) Low-frequency envelope, $E(t)$, of the stimulus, taken as the amplitude of the analytic signal via the Hilbert transform. (C) Input, $I(t)$, to a P-unit. (D) Raster plot of spike trains from 20 realizations. (E) Spike train from one realization of one single model P-unit. (F) Interspike interval histogram from the P-unit firing in the presence of the amplitude-modulating narrowband signal on the EOD.

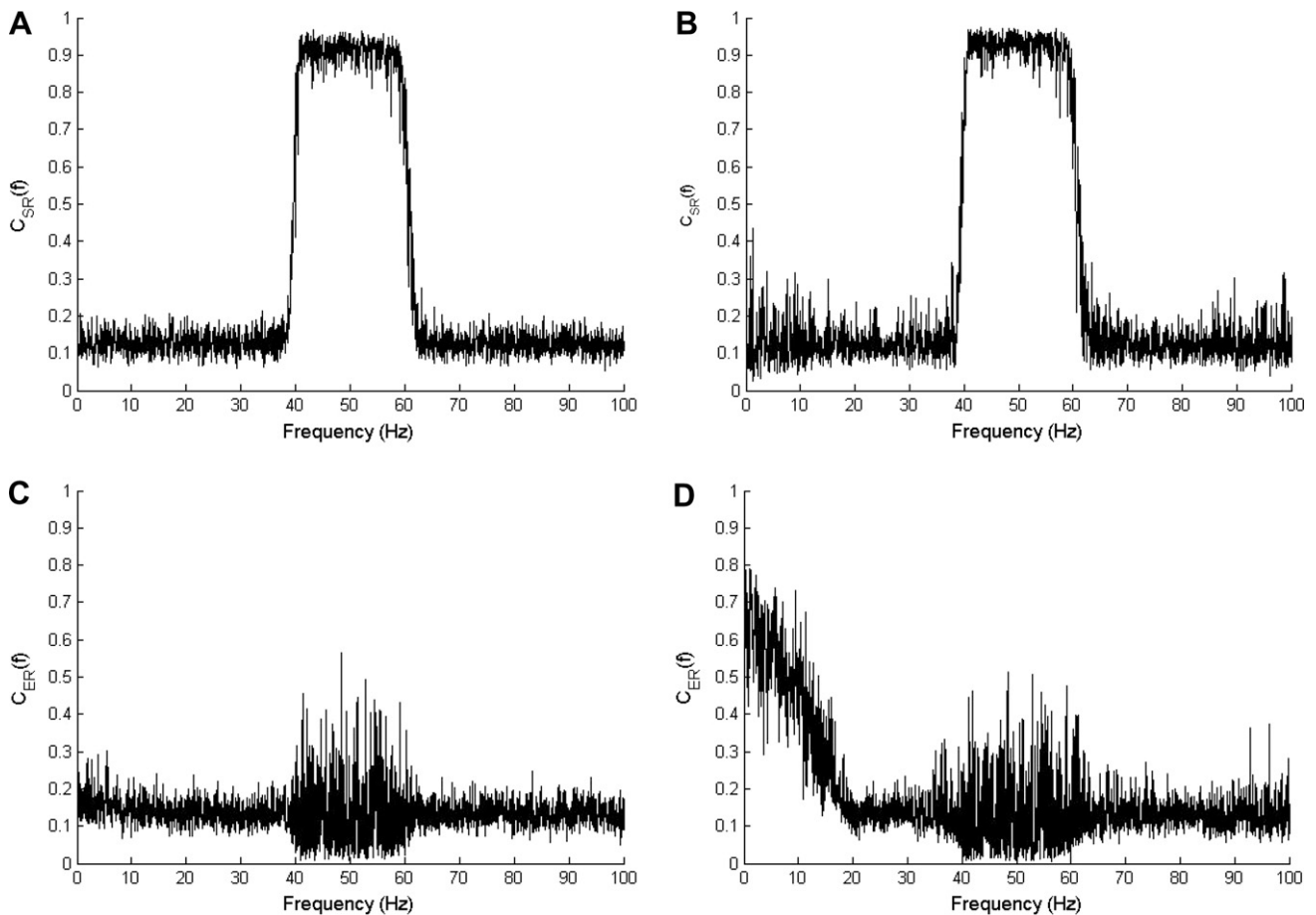


Fig. 15. Coherence estimates, averaged over 20 realizations, between the spike train response, $R(t)$, and (A and B) the stimulus, $S(t)$, leading to $C_{SR}(f)$, and (C and D) the envelope, $E(t)$, leading to $C_{ER}(f)$. Standard deviation of $S(t)$ at (A and C) 15% and (B and D) 30% of EOD amplitude.

clear from the spike times in Fig. 14 that firings occur mainly on the crests of the narrowband signal; they are not correlated so much with the envelope (a longer data set would make this point clearer). This point is obvious from Fig. 15A and C, where the P-unit codes for the narrowband signal (good S–R coherence in Fig. 15A), but not its envelope (poor E–R coherence in Fig. 15C). The values of coherence are very similar to the ones found experimentally. Fig. 15B and D are obtained for the same system except the stimulus contrast is twice as strong. Interestingly, E–R coherence now becomes appreciable, as seen from the increase in the 0–20 Hz band. This illustrates that nonlinearity in the f – I characteristic can be expressed by a larger stimulus which explores more of this f – I curve. In summary, the novel analysis presented here shows that this model reproduces experimental results on baseline firing statistics and envelope coding qualitatively and quantitatively.

7. Conclusion

We have presented an analysis of envelope encoding in a sensory pathway. The mechanism we have exposed [20,21], and detailed herein, is based on low-noise peri-threshold

processing. If the cell doing the extraction is further expected to transmit information only about the slow envelope, then it can do so using a slow synapse. This is what the ovoid cell does via its slow $GABA_B$ connection to the pyramidal cell in the electrosensory system. It could also send the narrowband signal with good linear encoding qualities through a fast synapse, but this requires that it behave linearly, which is not the case under the low-noise peri-threshold conditions for envelope transmission. So in some sense the transmission of direct signal or envelope are at odds with one another. *The electrosensory system solves this problem by sending the narrowband signal directly to the pyramidal cells, and the envelope comes via the ovoid cells.*

This coding is naturally applicable to carrier-based sensory systems, where the lower-frequency envelope can be extracted. In the case of the electrosensory system, we presented an even more elaborate context in which the mixture of high-frequency EOD's of interacting fish produces a narrowband mixture of moderate beat frequencies which are transmitted by the electroreceptors (and the EOD's themselves are not transmitted); this narrowband mixture has a higher-order feature in the form of a low-frequency envelope. It is clear however that the mechanism does not

require a carrier to begin with: any narrowband signal will have an envelope that could be extracted by this mechanism. The results are thus applicable to non-carrier-based senses as well, and to other parts of the brain, sensory or other, remotely located with respect to primary receptors.

The single LIF model can be made to extract envelopes of narrowband signals if the noise is low and the signal is peri-threshold. In this case it behaves similarly to the single pyramidal cells *in vitro* (not shown: see [21]) used to study envelope extraction. These cells were used to study the dynamics of the firing mechanism that lead to envelope extraction, even though in the real fish, this extraction has been shown to occur in the ovoid cells which connect to the pyramidal cells via a slow interneuron. This is because it is simpler to record from these pyramidal cells *in vitro*, without the confounding effects of realistic synaptic input. In particular, such input will add much noise, and consequently will make it difficult for such a cell to extract envelopes *in vivo*. This is why the pyramidal cells are not able to extract envelopes on their own *in vivo*, but rely on an indirect feedforward pathway via the ovoids. This enables them to respond to the direct signal as well, and with good coherence.

We have also shown results for an LIF model with dynamic threshold for the P-unit afferents (i.e. the electroreceptors). This model requires noise to produce the stochastic phase-locked firing characteristic of the baseline activity. This model has a smooth $f-I$ curve (not shown) due to the noise, and furthermore, it processes signals in its suprathreshold regime – in fact Fig. 13 shows that without any input the cell fires periodically in a phase locked manner. Consequently, this cell is not expected to do envelope extraction, but is expected to respond to the direct narrowband input. This is indeed what Fig. 15 reveals. This is also manifest in Fig. 14, where the spike train is seen to care more about (i.e. to do better rate-coding of) the narrowband modulations rather than the slow modulations of the envelope. This qualitative and quantitative agreement with experiment for both baseline firing statistics and S–R/E–R coherence required that the model be put into a more linear regime, by sufficiently reducing the stimulus contrast, or by increasing noise intensity and/ or current bias beyond threshold (data not shown).

Many species of weakly electric fish exhibit a jamming avoidance response, in which interacting fish move their respective EOD frequencies until a more comfortable separation is reached. What is the measure used by the fish to stop changing their frequencies, beyond the obvious desire to achieve a higher frequency beat? Does this have to do with the envelope power being somehow minimized? Is there an optimal modulation depth for the beat? Is it in the precise way that beats interfere with communication signals such as small and large chirps? Answers to these questions may also depend on the naturalistic amplitude and phase stimulation on the fishes' bodies, which is currently under closer scrutiny [16].

Further, what underlies the maximal sensitivity of the JAR? In *Eigenmannia* for example, the maximal response of the JAR occurs for frequency differences of 5 Hz or so. The reasons for this maximal sensitivity are not known. It would be interesting to correlate the ability to extract envelopes with the features of the jamming avoidance response. Likewise future work could also explore how the fish can actually behave in the detection experiment based on the set-up of Figs. 10 and 11. How is the response to a simple low-frequency stimulus impaired by envelope power? Hopefully we will obtain behavioral and electrophysiological answers to this question. Finally it will be crucial to build more realistic models of the electroreceptors coupled to the pyramidal and ovoid cells, to understand how more realistic features, such as intrinsic interval correlations in the receptor firing activity or the synaptic input and its plasticity, can reveal more surprises about parallel coding of signals and their envelopes and other multiscale spatiotemporal inputs.

References

- [1] D. Babineau, J.E. Lewis, A. Longtin, Spatial acuity and prey detection in weakly electric fish, *PLoS Comp. Biol.* 3 (2006) e38.
- [2] C.L. Baker Jr., *Current Opin. Neurobiol.* 9 (1999) 461.
- [3] J. Bastian, Electrolocation I. How the electroreceptors of *Apteronotus leptorhynchus* code for moving objects and other external stimuli., *J. Comp. Physiol.* 144 (1981) 465.
- [4] J. Benda, A. Longtin, L. Maler, A synchronization–desynchronization code for natural communication signals, *Neuron* 52 (2006) 347.
- [5] N.J. Berman, L. Maler, Neural architecture of the electrosensory lateral line lobe: adaptations for coincidence detection, a sensory searchlight and frequency-dependent adaptive filtering, *J. Exp. Biol.* 202 (1999) 1243.
- [6] C.E. Carr, M.A. Friedman, Evolution of time coding systems, *Neural Comput.* 11 (1999) 1.
- [7] M.J. Chacron, A. Longtin, M. St-Hilaire, L. Maler, Suprathreshold stochastic firing dynamics with memory in P-type electroreceptors, *Phys. Rev. Lett.* 85 (2000) 1576.
- [8] M.J. Chacron, K. Pakdaman, A. Longtin, Interspike interval correlations, phase locking and chaotic dynamics in a leaky integrate-and-fire model with dynamic threshold, *Neural Comput.* 15 (2003) 253.
- [9] M.J. Chacron, Nonlinear information processing in a model sensory system, *J. Neurophysiol.* 95 (2006) 2933.
- [10] D.R. Chialvo, How we hear what is not there: a neural mechanism for the missing fundamental illusion, *Chaos* 13 (2003) 1226.
- [11] D. Chialvo, A. Longtin, J. Mueller-Gerkin, Stochastic resonance in models of neuronal ensembles, *Phys. Rev. E* 55 (1997) 1798.
- [12] F. Gabbiani, Coding of time-varying signals in spike trains of linear and half-wave rectifying neurons, *Network Comp. Neural Syst.* 7 (1996) 61.
- [13] T.J. Gardner, M.O. Magnasco, Sparse time–frequency representations, *Proc. Nat. Acad. Sci. USA* 103 (2006) 6094.
- [14] W. Heiligenberg, *Neural Nets in Electric Fish*, MIT Press, Cambridge, MA, 1991.
- [15] P.X. Joris, C.E. Schreiner, A. Rees, Neural processing of amplitude modulated sounds, *Physiol. Rev.* 84 (2004) 541.
- [16] M. Kelly, A. Longtin, J.E. Lewis, Electric field interactions in pairs of electric fish: implications for conspecific localization, *Biol. Cybern.* (2008) in press.
- [17] B. Lindner, L. Schimansky-Geier, A. Longtin, Maximizing spike train coherence and incoherence in the leaky integrate-and-fire model, *Phys. Rev. E* 66 (2002) 031916.

- [18] A. Longtin, M. St-Hilaire, Encoding carrier amplitude modulations via stochastic phase synchronization, *Intern. J. Bifurc. Chaos* 10 (2000) 2447.
- [19] I. Mareschal, C.L. Baker Jr., *Nat. Neurosci.* 1 (1998) 150.
- [20] J.W. Middleton, A. Longtin, J. Benda, L. Maler, The cellular basis for parallel neural transmission of a high-frequency stimulus and its low-frequency envelope, *Proc. Nat. Acad. Sci. USA* 103 (2006) 14596.
- [21] J.W. Middleton, E. Harvey-Girard, L. Maler, A. Longtin, Envelope gating and noise shaping in populations of noisy neurons, *Phys. Rev. E* 75 (2007) 021918.
- [22] M.E. Nelson, Z. Xu, J.R. Payne, Characterization and modeling of P-type electrosensory afferent responses to amplitude modulations in a wave-type electric fish, *J. Comp. Physiol. A* 181 (1997) 532.
- [23] Z.M. Smith, B. Delgutte, A.J. Oxenham, Chimaeric sounds reveal dichotomies in auditory perception, *Nature* 416 (2002) 87.
- [24] M. St-Hilaire, A. Longtin, Coding of information in models of tuberosus electroreceptors, *Math. Biosci.* 188 (2004) 157.
- [25] C. van Vreeswijk, in: C. Chow, B. Gutkin, D. Hansel, C. Meunier, J. Dalibard (Eds.), *Methods and models in neurophysics, Lecture Notes of the Les Houches Summer School 2003*, Vol. LXXX, Elsevier, Amsterdam, 2005, p. 345.
- [26] R. Wessel, C. Koch, F. Gabbiani, Coding of time-varying electric field amplitude modulations in a wave-type electric fish, *J. Neurophysiol.* 75 (1996) 2280.
- [27] H.H. Zakon, The electroreceptive periphery, in: T.H. Bullock, W. Heiligenberg (Eds.), *Electroreception*, John Wiley and Sons, New York, 1986, p. 103.